BEILSTEIN ARCHIVES

This open access document is posted as a preprint in the Beilstein Archives at https://doi.org/10.3762/bxiv.2021.67.v1 and is considered to be an early communication for feedback before peer review. Before citing this document, please check if a final, peer-reviewed version has been published.

This document is not formatted, has not undergone copyediting or typesetting, and may contain errors, unsubstantiated scientific claims or preliminary data.

Preprint Title Synthesis, characterization, and cytotoxic evaluation of iron oxide nanoparticles functionalized with galactomannan

Authors Francisco R. S. Mendes, Fernanda N. Rodrigues, Nidyedja G. G. Gonçalves, Mateus T. Aerre, Kelvi W. E. Miranda, Francisco F. Bezerra, Paulo A. S. Mourão, Ana C. O. Monteiro-Moreira, Maria S. R. Bastos, Huai N. Cheng, Atanu Biswas, Antônio C. H. Barreto, Hélcio S. dos Santos, Alexandre M. R. Teixeira and Renato A. Moreira

Publication Date 24 Sep 2021

Article Type Full Research Paper

Supporting Information File 1 Supplementary Material_FeNP_Gal_S_BJNANO.docx; 278.9 KB

ORCID® iDs Francisco R. S. Mendes - https://orcid.org/0000-0001-8357-6707; Fernanda N. Rodrigues - https://orcid.org/0000-0001-6099-0008; Nidyedja G. G. Gonçalves - https://orcid.org/0000-0002-7416-1005; Kelvi W. E. Miranda - https://orcid.org/0000-0002-5932-4996; Ana C. O. Monteiro-Moreira - https://orcid.org/0000-0002-3606-6808; Huai N. Cheng - https://orcid.org/0000-0001-8647-057X; Antônio C. H. Barreto - https://orcid.org/0000-0002-5757-334X; Hélcio S. dos Santos - https://orcid.org/0000-0001-5527-164X; Alexandre M. R. Teixeira - https://orcid.org/0000-0001-6786-2076

License and Terms: This document is copyright 2021 the Author(s); licensee Beilstein-Institut.

This is an open access work under the terms of the Creative Commons Attribution License (https://creativecommons.org/licenses/by/4.0). Please note that the reuse, redistribution and reproduction in particular requires that the author(s) and source are credited and that individual graphics may be subject to special legal provisions. The license is subject to the Beilstein Archives terms and conditions: https://www.beilstein-archives.org/xiv/terms. The definitive version of this work can be found at https://doi.org/10.3762/bxiv.2021.67.v1

Synthesis, characterization, and cytotoxic evaluation of iron oxide nanoparticles functionalized with galactomannan

Francisco R.S. Mendes[1,9], Fernanda N. Rodrigues[4], Nidyedja G.G. Gonçalves[4], Mateus T. Aerre[3], Kelvi W.E. Miranda[5], Francisco F. Bezerra[6], Paulo A. S. Mourão[6], Ana C.O. Monteiro-Moreira[1,3], Maria S.R Bastos[2], Huai N. Cheng[7], Atanu Biswas[8], Antônio C.H. Barreto[10], Hélcio S. dos Santos[1,9], Alexandre M.R. Teixeira[1, *9], Renato A. Moreira[1,3,4]

Address: [1] Graduate Program in Biotechnology, Northeast Biotechnology Network, State University of Ceará, Campus Itaperi, Fortaleza, CE, Brazil.
[2] Food Packaging Technology Laboratory, Embrapa Agroindústria Tropical, Fortaleza, CE, Brazil.
[3] Centre of Experimental Biology (NuBEx), University of Fortaleza, Fortaleza, CE, Brazil.
[4] Department Biochemistry and Molecular Biology, Federal University of Ceará, Fortaleza, CE, Brazil.
[5] Graduate Program in Biomaterials Engineering, Federal University of Lavras, Lavras, MG, Brazil.
[6] Institute of Medical Biochemistry Leopoldo de Meis, University Hospital Clementino Fraga Filho, Federal University of Rio de Janeiro, 21941-913 Rio de Janeiro, RJ, Brazil.
[7] USDA Agricultural Research Service, Southern Regional Research Center, 1100 Robert E. Lee Blvd., New Orleans, LA 70124, USA.
[8] USDA Agricultural Research Service, National Center for Agricultural Utilization Research, 1815 N. University St., Peoria, IL 61604, USA.
[9] Graduate Program in Biological Chemistry, Department of Biological Chemistry, Regional University of Cariri, Crato, CE, Brazil.
[10] Department of Physics, Federal University of Ceará, Fortaleza, CE, Brazil.

Email: Alexandre M.R. Teixeira – alexandre.teixeira@urca.br

* Corresponding author

Abstract

Iron nanoparticles (FeNP) present excellent magnetic properties and chemical stability, and for this reason, they are often configured into materials for a variety of potential uses in medical, biotechnological, and other applications. In this work, iron oxide nanoparticles functionalized with galactomannan (FeNP/Gal) from *Caesalpinia pulcherrima* were synthesized and submitted to characterization and evaluation of the cytotoxic activity. The functionalized nanoparticles were synthesized by co-precipitation and subjected to a process of surface modification with galactomannan and epichlorohydrin. These nanomaterials were characterized using infrared spectroscopy, X-ray diffraction (XRD), thermogravimetric analysis (TGA), differential thermogravimetric analysis (DTA), and scanning electron microscopy (SEM). 1D and 2D nuclear magnetic resonance (NMR) spectroscopy were also used in the structural analysis of the galactomannan. In addition, i*n vitro* study was carried out to evaluate the cytotoxic activity of the FeNP/Gal nanoparticles on human cells of the HEK-293 strain (ATCC® CRL-1573). The FeNP/Gal nanoparticles had an average diameter of 13 ± 2 nm as opposed to 11 ± 2 nm for unreacted FeNP. The infrared spectrum of the FeNP/Gal nanoparticles presents characteristic absorbance bands of their chemical constituents, confirming that the iron oxide nanoparticles were functionalized with galactomannan. The cytotoxicity assay for the FeNP/Gal nanoparticles did not show significant cytotoxicity against HEK 293-Human embryonic kidney cell lines below 800 µg/mL However, this study points out the possibility of using hemicellulose and other plant-based polysaccharides to produce nanostructured materials for tissue engineering and other biomedical applications.

Keywords

Functionalized nanoparticles; Galactomannan; XRD; TGA; DTA; SEM.

Introduction

Nanoparticles of inorganic materials have been the focus of recent research attention due to their magnetic properties, chemical stability, and structural dimensions that render them suitable for medical and biotechnological applications [1]. These nanomaterials have been shown to be useful in microfluidics [2], photonics [3], Li-ion batteries, catalysis [1], chemical sensors [4], magnetic separation [5], and biomedical applications [6].

Magnetic iron oxides (e.g., Fe_3O_4 and γ-Fe_2O_3) with different nanostructures are involved in biomedicine, such as contrast agents in magnetic resonance, drug release agents, and specific materials for cell imaging and biomedical treatments [7]. More specifically, these innovative materials are considered model systems for fluid magnetic hyperthermia in the treatment of cancer. For chemotherapy and radiotherapy, their properties, such as superparamagnetism and chemical stability, are especially beneficial [7]. Nonetheless, biocompatibility and biodegradability of the materials used are potentially important for applications in the fields of biomedicine and tissue engineering [5, 6].

Caesalpinia pulcherrima of the genus Caesalpinia belongs to the family Leguminosae-Caesalpinioideae and is popularly known as flamboyant-de-jardin or flamboianzinho [8]. This species has the shape of a woody shrub, and its fruit has a variant size of about 6 to 12 cm in length [8]. This plant multiplies itself with seeds, which are produced in the semiarid region of Northeast Brazil, mainly in the state of Ceará [9]. The seeds are rich in galactomannan (a type of hemicellulose), which has a chemical

structure consisting of a main chain of D-mannopyranose linked together with β- (1 → 4) bonds, with branches of D-galactopyranose linked via α-(1 → 6) onto the main-chain mannopyranose [10-12]. This biopolymer seems promising for use in controlled drug release [13, 14]. For water-soluble drugs, the release of the drug can be controlled according to the degree of cross-linking in this biopolymer [15]. In addition, it has been used in the formulation of hydrogels and cross-linking of membranes for wound healing [16], as well as in the development of new food packaging materials [11, 17]. The galactomannans are sustainable, biodegradable, and ecofriendly polymers that can be combined with magnetic nanomaterials in order to reduce the toxicity of the nanomaterials [18].

In view of the above considerations, the present work was aimed to synthesize iron oxide nanoparticles and functionalize them with the hemicellulose biopolymer extracted from the seeds of *Caesalpinia pulcherrima*. These functionalized nanoparticles were then characterized and evaluated for *in vitro* cytotoxicity, using normal human HEK-293 cells (ATCC® CRL-1573).

Results and Discussion

Biopolymer extraction and characterization

The extraction yield of the polysaccharide from the seeds was expressed as the percentage of dry weight obtained after extraction in relation to the dry weight of the seeds [19]. The extraction of galactomannan from *C. pulcherrima* showed a yield of 25% (w/w) in relation to the seed weight. The literature reported similar results for the extraction of biopolymers in seeds of *G. triacanthos* and *C. pulcherrima*, which showed yields of 24.73% and 25%, respectively [11, 20].

The galactomannan showed a Mw of 4.3 x 10^6 g.mol^{-1} and a Mn of 3.8 x 10^5 g.mol^{-1}. In earlier work, the molecular weights were shown to be 1.34 x 10^7 [12]. The Mw/Mn polydispersity was 11.3. During the synthesis of this biopolymer, the mannosyl transferase enzyme influenced and regulated the size of the biopolymer chain [21].

The ^{1}H NMR and ^{1}H-^{13}C HSQC spectra of the galactomannan are shown in Figures S1 and S2 of the Supplementary Material, respectively. The NMR data are consistent with the galactomannan structure, with the ^{1}H and ^{13}C peaks assigned in the figure. The ratio of galactose : mannose appears to be about 1: 1.8 [11]. Thus, this galactomannan is similar to guar gum, which is approved for use as a thickener and stabilizer in food and feed formulations.

Characterization of nanoparticles

In order to evaluate the functionalization of inorganic materials by organic molecules, such as biopolymers, different analytical techniques need to be used [22]. The surface modification of the nanoparticles can be seen in the IR spectra, shown in Figure 1. The unmodified iron oxide nanoparticle (FeNP) spectrum shows wide bands at 3400-3030 cm^{-1} for O-H stretching [23, 24] and a relatively narrow 1624 cm^{-1} band attributed to the bending vibrations for the water molecules coordinated with Fe atoms on the surface [23, 24]. The bands at <700 cm^{-1} are all due to the vibrations of Fe-O bonds. For example, the band at 630-550 cm^{-1} can be attributed to the vibrations of Fe-O bonds of iron oxide in the tetrahedral and octahedral structures of the Fe_3O_4 crystals [23]. The 432 cm^{-1} band is due to the octahedral site and corresponds to the Fe-O bond of the magnetite [23, 25].

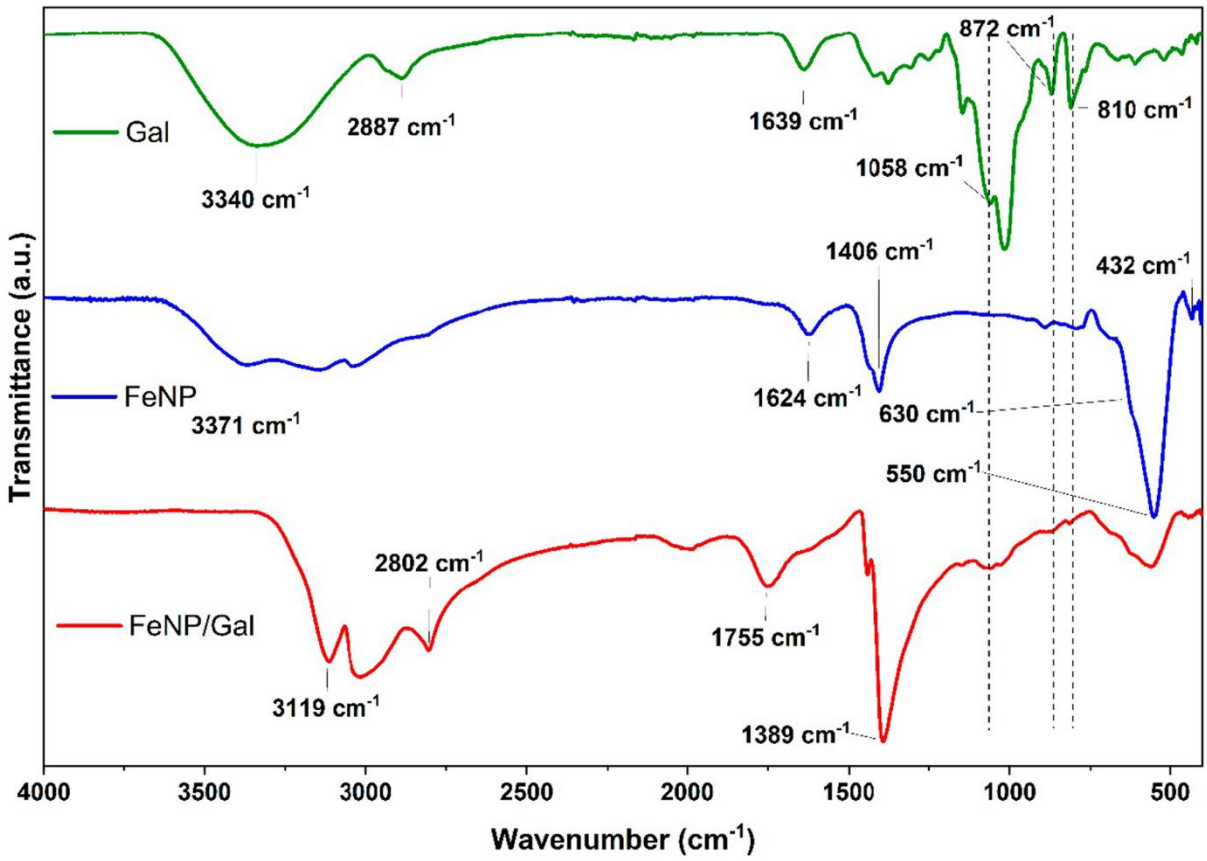

Figure 1: FT-IR spectra of the samples of galactomannan (Gal), iron nanoparticles (FeNP) and iron nanoparticles functionalized with galactomannan (FeNP/Gal).

The FT-IR spectrum of the samples of galactomannan (Gal) (Figure 1, top) shows an intense absorption band at 3340 cm^{-1} assigned to the O-H stretching vibration [26, 27]. The band at 2884 cm^{-1} can be attributed to the C-H symmetric and asymmetric vibrations [26, 27]. The band at 1639 cm^{-1} is due to the residual water present [28] and possibly COO^- asymmetric stretching [29]. The intense band at 1058 cm^{-1} is associated with the vibrations of C-O-C in the pyranose ring [30]. The bands at 872 and 810 cm^{-1} correspond to the stretching in the anomeric conformations β-D-mannopyranose and α-D-galactopyranose, respectively [26, 27, 30].

The FT-IR spectrum of FeNP/Gal nanoparticles (Figure 1, bottom) provides the imprints of the chemical reactions involved. In the region 1300-4000 cm^{-1}, the IR spectrum is somewhat similar to that of epichlorohydrin itself [31], but below 1300 cm^{-}

[1], the bands corresponding to epichlorohydrin are much diminished in intensities, suggesting that a part of the epichlorohydrin has reacted. Even better understanding can be obtained by a comparison with the FT-IR spectra of epichlorohydrin, ethylene oxide, and 1,2-dichloroethane [31] and the earlier assignments for epichlorohydrin as published in the literature [32, 33]. Thus, the bands at 3119 and 3000 cm^{-1} are due to epoxide vibrations of the C-H stretching modes, and the band at 1389 cm^{-1} may be attributed to CH_2Cl deformations. The band at 550 cm^{-1} confirms the presence of iron oxide; the absence of the OH bands at 3200-3500 cm^{-1} suggests that the OH groups on iron oxide have mostly reacted with epichlorohydrin or Gal. The band at 1755 cm^{-1} (for carbonyl functionalities) suggests that perhaps some of the epoxides have been rearranged to carbonyl functionalities [34, 35]. The band at 2802 cm^{-1} and the small band at 1050 cm^{-1} indicates the presence of galactomannan that is attached to iron oxide or epichlorohydrin residues, but the absence of the OH band at 3340 cm^{-1} suggests that the amount of galactomannan is either relatively low and/or that the OH in galactomannan has mostly reacted with epichlorohydrin or iron oxide. An approximate reaction scheme below roughly captures the situation:

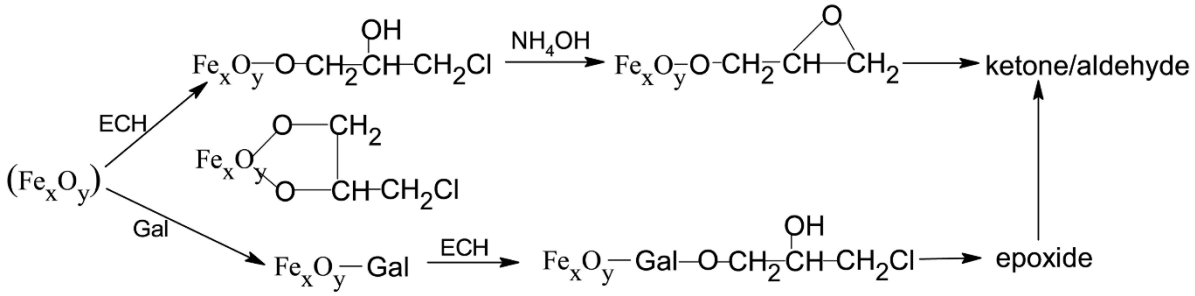

Scheme 1. Reaction pathways where iron oxide (Fe_xO_y) was formed in situ, in the presence of epichlorohydrin (ECH) and galactomannan (Gal).

Note that the IR spectrum observed for FeNP/Gal in this work is different from the spectra reported earlier for iron oxide nanoparticles coated with dextran [36, 37]. In those cases, the dextran was reacted with epichlorohydrin and NaOH, which caused cross-linking of the dextran. In our reaction of Gal with epichlorohydrin, NaOH was not used. As a result, less Gal was incorporated in the FeNP/Gal nanoparticles, and less cross-linking took place. Our method was designed under conditions such that the reaction medium promoted FeNP synthesis and functionalization in one step.

Dynamic light scattering (DLS) can be used to determine the average size of the nanoparticles in the liquid phase, based on the Brownian motion of the particles, which is inversely proportional to the particle diameter [38]. **Table 1** shows the average diameters of 240 nm (for FeNP), 332 nm (for FeNP/Gal), and 182 nm (for Gal). The sizes for all three materials exhibited Gaussian distributions (results not shown). The increase in particle size observed for FeNP/Gal relative to FeNP was due to the reactions of Gal and epichlorohydrin on iron oxide and the possible formation of aggregates between the magnetic nanoparticles and the biopolymer, although intermolecular hydrogen bonding [39] and intermolecular forces [40] (e.g., Van der Waals, capillary and electrostatic forces) can also be active in the aqueous medium [39-41].

Table 1: Size of iron oxide nanoparticles produced from co-precipitation measured by dynamic light scattering (DLS) and zeta potential (ζ).

Treatament	**Average diameter (nm)**	**ζ (mV)**
Gal	182.0 ± 0.2*	-12.20 ± 1.7
FeNP	240.0 ± 12.0	16.70 ± 0.80
FeNP/Gal	332.0 ± 38.0	-30.00 ± 1.40

* Hydrodynamic radius (HR).

Table 1 also gives the zeta potential (ζ): 16.70 ± 0.8 mV (for FeNP), -12.20 ± 1.7 (for Gal) and -30.00 ± 1.40 mV (for FeNP/Gal). FeNP/Gal showed an increase in stability in an aqueous solution relative to FeNP and Gal solution [25, 42]. This confirms the presence of some carboxylic groups possibly formed during the drying step during the preparation of the material. In this case, a shoulder band at 1700 cm^{-1} was observed in the IR, corresponding to COO asymmetric stretching [29]. Thus, the surface of the nanoparticles was at least partly covered by galactomannan.

X-ray diffraction is a technique used to determine the structural properties of many organic and inorganic materials [43]. It allows the identification of crystalline compounds, network parameters, crystalline grain size, and preferred orientation and degree of crystallinity of the materials [43, 44]. The galactomannan diffractogram, Figure 2A, shows an amorphous structure. However, it also contains a small amount of partially crystalline regions formed by the packing of mannan chains in the less substituted regions of the biopolymer [26].

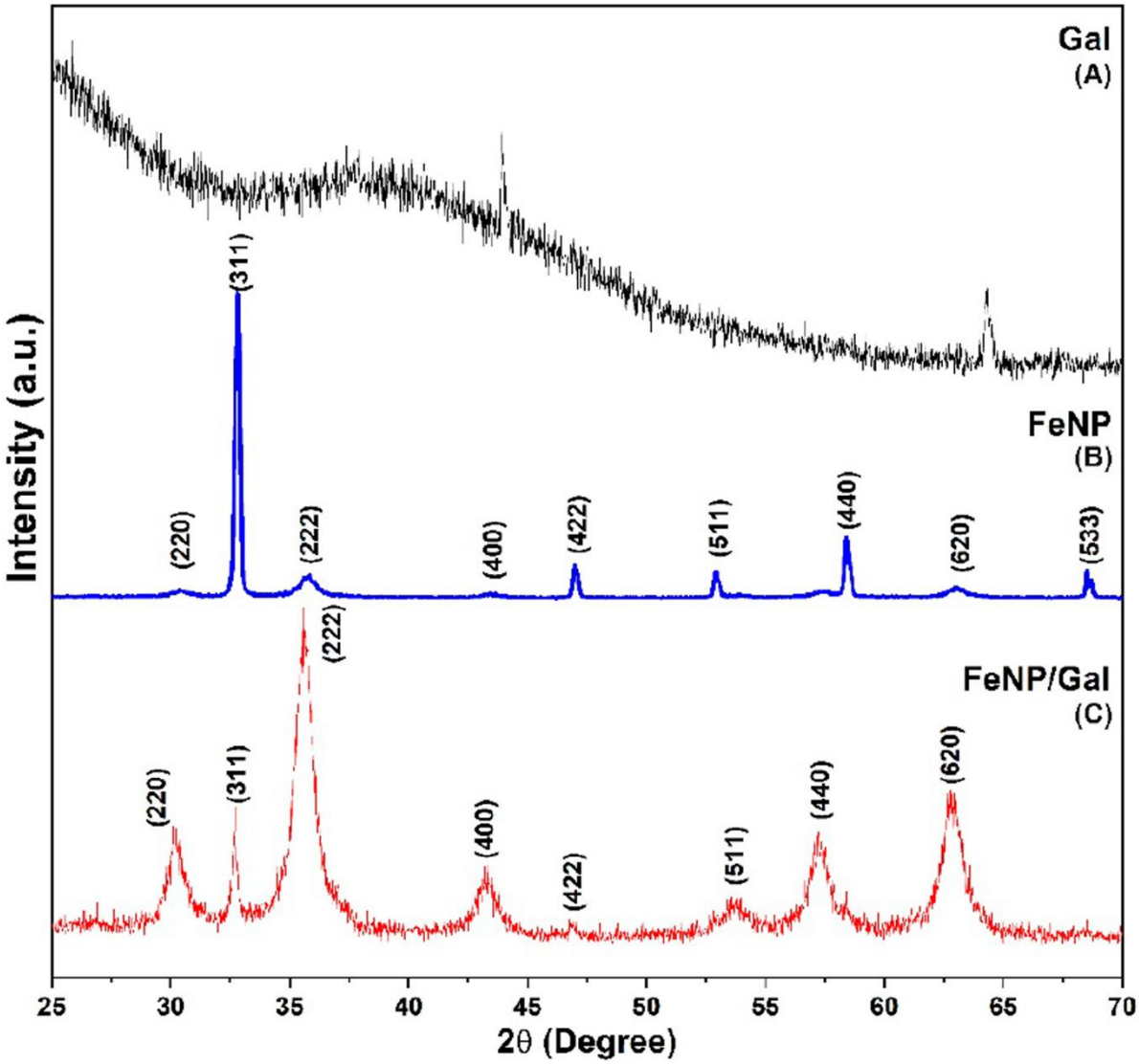

Figure 2: XRD diffractograms of the samples (A) Gal, (B) FeNP, and (C) FeNP/Gal.

The FeNP diffractogram, Figure 2B, shows that the nanomaterial is crystalline. In the literature, the direction of crystallite growth is along the planes that are characteristically observed in iron oxide (220), (311), (222), (400), (422), (511), (440), (620), and (533) [45]. The diffraction peaks are consistent with the observations made in the IR spectrum (Figure 1) for Fe_3O_4 nanoparticles with the presence of peaks characteristic of the vibrations at 600-550 cm^{-1}. Thus, the XRD data are consistent with the presence of magnetite, confirmed by the peaks at (220) and (311) [46]. The XRD pattern is very close to the reported data in JCPDS 65-3107 [47].

In Figure 2C, the iron nanoparticles reacted with galactomannan and epichlorohydrin show broadening of the diffraction peaks for iron oxide, reflecting the coating of the magnetic nanoparticle with organic materials. In this case, the diffractogram for FeNP remained essentially unchanged after galactomannan-epichlorohydrin reaction, e.g., the diffraction peaks at (220), (311), (400), (422), (511), and (440), which are characteristic of Fe_2O_3. Furthermore, all the peaks shown suggested a mixture of maghemite Fe_2O_3, residual γ-Fe_2O_3, and magnetite Fe_3O_4 [45]. The observation can be attributed to the fact that magnetite and maghemite have a cubic structure with very similar network parameters [48]. The efficient coating process on iron oxide nanoparticles can be seen in Figure 2, where the contribution of amorphous areas causes enlargements and reductions of intensities in most peaks. Moreover, the amorphization causes some displacements of the peaks, as observed at 2θ = 43.4° and 63.0°, which shift to 2θ = 44° and 64°). However, the diffractogram does not present any loss of nanomaterial crystallinity, indicating that the internal structure of FeNP is maintained. Therefore, DLS data together with XRD result confirm that the nanoparticles are coated with galactomannan and epichlorohydrin derivatives. The thermal properties of the materials have been evaluated by TGA. With this technique, we can determine the composition of FeNP/Gal and possible interactions of the components [49]. Figure 3 shows the thermal degradation of FeNP, Gal, and FeNP/Gal, which displays two or more main weight-loss stages from 25 to 700 °C.

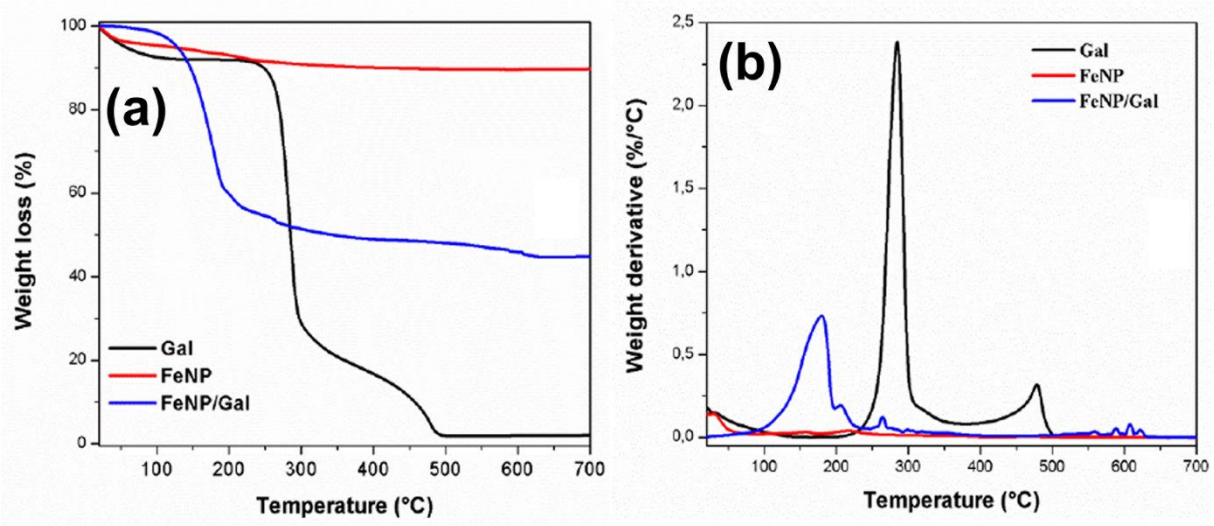

Figure 3: (A) Thermogravimetric curves for Gal, FeNP and FeNP/Gal, and (B) differential thermogravimetric curves for the same samples.

In the first stage, the loss of weight is mainly due to the elimination of water molecules absorbed by the material(s) or adsorbed on the surface [50]. The weight losses are 8.0% (Gal), 4.4% (FeNP), and <0.5% (FeNP/Gal). This result is compatible with the IR data, where the water bending vibration was observed at 1630 cm^{-1} for Gal and FeNP (Figure 1). Similar results have been reported earlier [50], where the first stage of the thermal curve showed a loss of weight of around 3.0% in iron oxide nanoparticles at about 180 °C. In the second stage, weight losses of 64% and 48% were found for Gal and FeNP/Gal at 286 °C and 190 °C, respectively. For Gal, this was due to the breakdown of the polysaccharide structure, as shown for similar data for guar gum [51, 52]. However, in FeNP/Gal, the lower weight-loss temperature was due to the degradation of epichlorohydrin residues and Gal-epichlorohydrin residues attached to iron oxide, as shown in Scheme 1. In the third stage, 300-700°C, the degraded Gal was converted to aromatic structures and then to biochar. For FeNP/Gal, the weight loss at > 380°C was relatively small (perhaps 4%), suggesting that the Gal content in FeNP/Gal was about 15-20%. From the residual weights at 500°C, the amount of iron

oxide in FeNP/Gal was about 50%. Thus, the amount of epichlorohydrin residues in FeNP/Gal was about 30-35%.

Microscopic analysis (FEG-SEM) can indicate, with subsequent high-resolution imaging techniques, the presence of clusters and the nanometric distribution of particle size [53]. The topography of coated and uncoated iron nanoparticles and the mean diameters are shown in Figure 4.

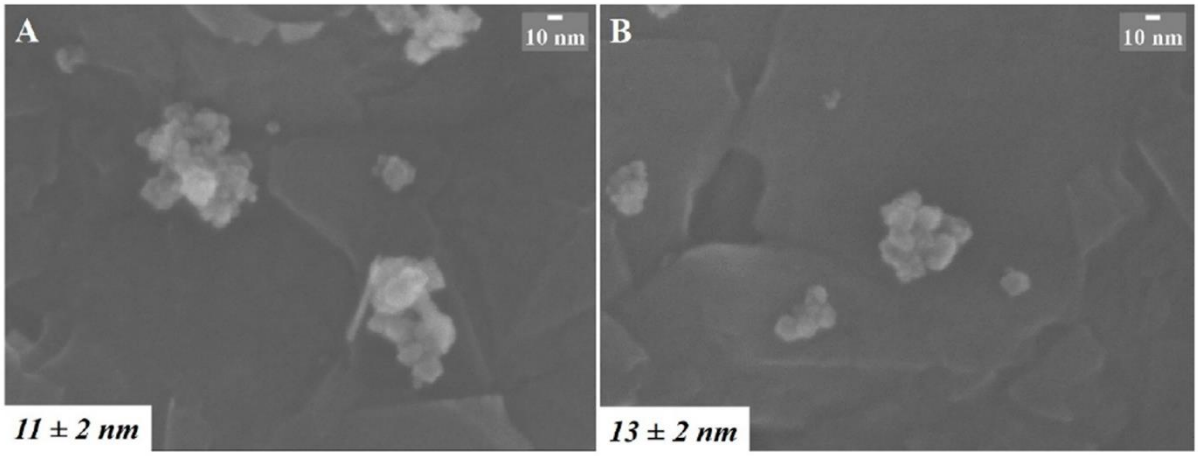

Figure 4: SEM micrographs for the (A) iron oxide nanoparticles (FeNP), and (B) iron oxide nanoparticle reacted with galactomannan and epichlorohydrin (FeNP/Gal). It is shown in the lower left corners are the average particle diameters (mean ± standard deviation, n = 100).

The photomicrographs indicate that the incorporation of the biopolymer on the FeNP resulted in an increase in diameter. FeNP had a mean diameter of around 11 nm. Similar results were observed in the literature, with the core diameter ranging from 10 to 20 nm [54]. With the incorporation of the biopolymer, the mean diameter increased to 13 nm due to the addition of organic matters, as shown in Scheme 1. Furthermore, the presence of the biopolymer led to the formation of imperfections in the morphology of the nanoparticles (Figure 4B) and the tendency for cluster formation because the nanoparticles functioned as small magnets that tended to attract each other.

Iron oxide nanoparticles are attractive for biomedical applications because they have controllable sizes ranging from a few nanometers to tens of nanometers. These dimensions are smaller or comparable to those of a virus (20-450 nm), a protein (5–50 nm), a gene (2 nm wide and 10–100 nm long), or a cell (10-100 µm) [55]. Thus, they can have the potential to enter or interact with a biological entity of interest. By coating these nanomaterials with biomolecules for connections or interactions with the biological entity, we have an additional tool to control or modify these interactions [56, 57].

Cytotoxicological assay of nanoparticles for HEK-293

FeNP and FeNP/Gal samples did not show a significant effect ($p = 0.0377$) on cell viability of the HEK-293 strain below the concentration of 800 µg/mL (Figure 5). For both nanoparticles at the tested concentrations, there was no significant difference in cell viability at concentrations greater than 25 $\mu g.mL^{-1}$. It is important to note that, at the concentrations evaluated, the nanoparticles in the culture medium did not interfere with the fluorescence readings. FeNP and FeNP/Gal exhibited an inhibitory concentration at 50% inhibition (IC50) above 800 $\mu g.mL^{-1}$.

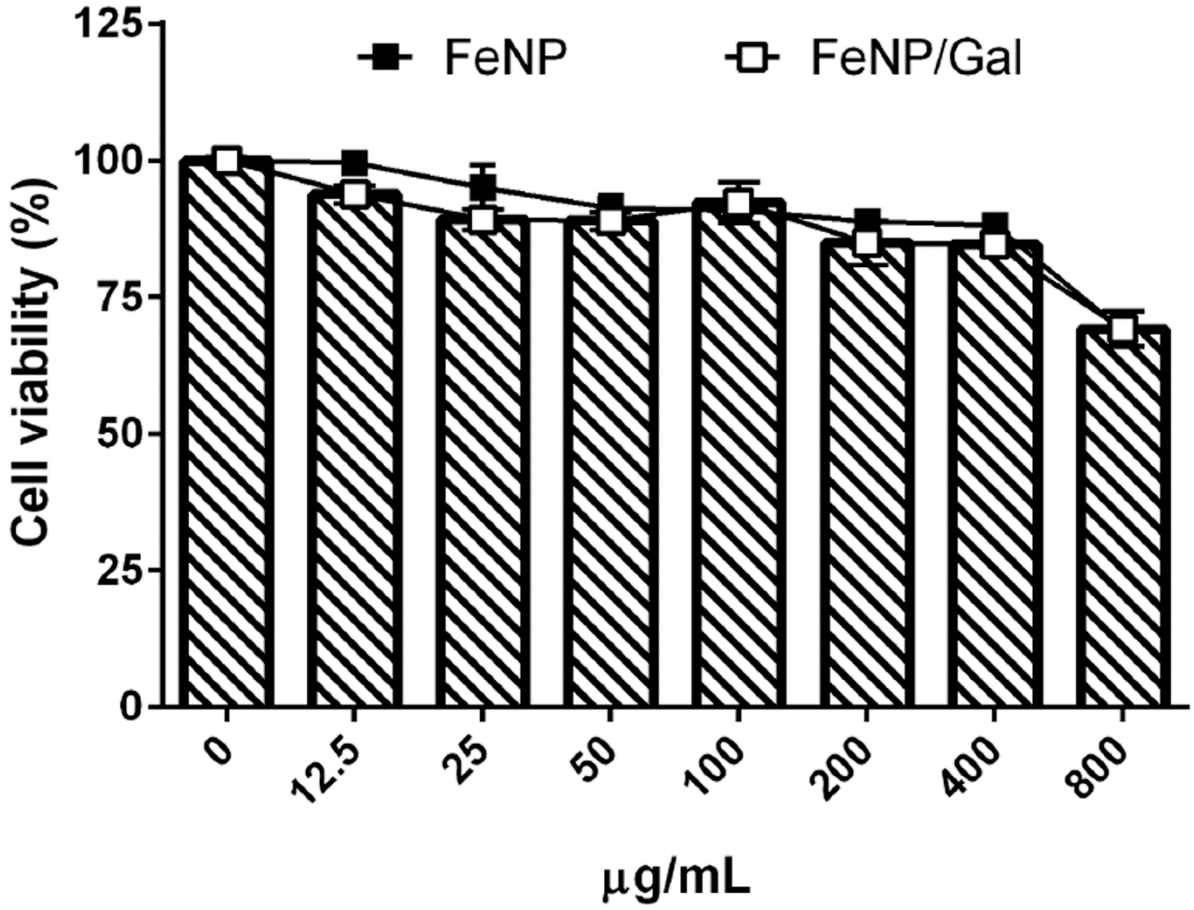

Figure 5: Viability of HEK-293 cells incubated with iron nanoparticles (FeNP) and iron nanoparticles with galactomannan (FeNP/Gal) at concentrations of 12.5 to 800 µg.mL^{-1}. Each value represents the mean ± standard error of the mean (E.P.M.)

Earlier studies showed that the mechanism of action of iron oxide nanoparticles is linked to the generation of reactive oxygen species (ROS), which can result in inflammatory processes in the cells and consequent rupture in the mitochondrial membrane, DNA damage, and programmed cell death due to apoptosis [58, 59]. However, the present result can be rationalized by the fact that the reactions caused by the iron ions generated by the dissociation of NPs in the cell cytoplasm are controlled by a complex of proteins that can transport or store this nanomaterial, thereby providing for the cell tolerance of FeNP.

Conclusion

The reaction of the iron oxide nanoparticles with epichlorohydrin and galactomannan (FeNP/Gal) was performed successfully. The reaction procedure for these iron nanoparticles is easy to use and can be scaled up to the production levels. The infrared spectrum of the FeNP/Gal nanoparticles presents characteristic absorbance bands of their chemical constituents, confirming that the iron oxide nanoparticles were functionalized with galactomannan. The nanoparticles obtained did not show cytotoxicity against the normal human cell line at the concentrations evaluated. The reaction with epichlorohydrin and galactomannan did not significantly change the morphology of the FeNP, increasing its mean diameter from 11 ± 2 nm to 13 ± 2 nm. The results of this work suggest that the FeNP/Gal can be used as a biomedical nanomaterial for many applications, e.g., direct surface contact with pathogenic micro-organisms, prevention or disruption of the formation of biofilms on devices, and environment/medical diagnostics. Moreover, this approach opens a new window for the design of magnetic nanoparticles in tissue engineering and other biomaterials through the choice of pertinent plant biopolymers and the modified coating procedure.

Experimental

Materials

Iron (III) chloride hexahydrate, iron (II) chloride heptahydrate, ammonium hydroxide (28–30%), and acetone (ACS reagent grade) were acquired from Sigma Aldrich Company, Milwaukee, WI, USA.

Extraction and characterization of biopolymer

The extraction of galactomannan was adapted from the procedure described by Cerqueira *et al.* [19]. Seeds were removed from the pods, cleaned, placed in a blender, and mechanically broken. Afterward, the endosperm was manually separated from the germ and the hull. The endosperm obtained was suspended in 96% ethanol (w/w) in a proportion of 1:3 (seeds: ethanol) at 70 °C for 20 min to inactivate the enzymes and eliminate the low-molecular-weight compounds. The ethanol was removed, and distilled water was added in a 1:10 (endosperm: water) proportion, and the suspension was left overnight. The next day, the amount of water was refilled to an endosperm: water ratio of 1:10 and mixed in a blender for 5 min. Next, the viscous solution was filtered through a nylon net and precipitated by adding 96:4 ethanol:water at a weight ratio of 1:2. The precipitate was successively washed with acetone, dried with hot air, and milled.

The molecular weights (Mn and Mw) of the biopolymer was determined by gel permeation chromatography (GPC) (Shimazu Model LC-20AD, Kyoto, Japan) using a PolySep linear column (7.8 x 300 mm, Waters, Milford, MA, USA), flow rate of 1.0 $mL.min^{-1}$, biopolymer concentration of 1 $mg.mL^{-1}$, and 0.1 $mol.L^{-1}$ $NaNO_3$ in water as the eluent. The elution volume was corrected using ethylene glycol as an internal marker at 11.25 mL. The GPC was calibrated with pullulan samples (Shodex, Showa Denko, Kawasaki, Japan) as standards. All analyses were conducted at room temperature. A Waters Model RID-10A (Milford, MA, USA) was used as the refractive index detector. The polydispersity value was calculated via M_w/M_n [11].

NMR spectra (1D and 2D) were acquired using 2.5% (*w*/*v*) solutions in D_2O on an Avance DRX 500 spectrometer (Bruker, Billerica, MA, USA). For the 2D ^{1}H-^{13}C HSQC experiment, we used 128 scans, 1024 x 256 points, GARP pulse decoupling, and a 2s

delay time between scans. For 2D ^{1}H-^{1}H NOESY spectra, 32 scans, 2048 x 512 points, and a 2s delay time between scans were used. The analysis was performed at a probe temperature of 323K using tetramethylsilane (TMS) as external reference (0.00 ppm).

Synthesis of nanoparticles by co-precipitation

Magnetic iron oxide nanoparticles (FeNP) were prepared by alkaline co-precipitation of ferrous chloride tetrahydrate, $FeCl_2.4H_2O$ (1.34 g), and ferric chloride hexahydrate $FeCl_3.6H_2O$ (3.40 g) at a 1:2 ratio. The salts were dissolved in 150 mL deionized water in a three-necked glass flask, which was placed in a heating mantle with a magnetic stirrer. When the salt solution was vigorously stirred at 70 ºC, ammonium hydroxide (NH_4OH) was added to the system dropwise. The black precipitate was washed with deionized water until the solution pH was 7.0. The solution was then centrifuged at 5000 rpm for 30 min. The precipitates were collected and dried in an oven at 50 ºC for 12 h [6].

Synthesis of galactomannan-coated magnetic iron oxide nanoparticles

Galactomannan-coated magnetic iron oxide nanoparticles (FeNP/Gal) were synthesized by the co-precipitation of Fe (II) and Fe (III) in the presence of 2 mL of epichlorohydrin molecules. Thus, 1.34 g $FeCl_2.4H_2O$ and 3.40 g $FeCl_3.6H_2O$ were dissolved in 100 ml of deionized water. Then 1 g of galactomannan previously dissolved in solution was added together with 2 mL epichlorohydrin. The final solution was then vigorously stirred at 2,000 rpm at 70 °C for 1 h. In the next step, NH_4OH solution at a concentration of 4 $mol.L^{-1}$ was added slowly to produce small-sized nanoparticles. The resulting dispersion was stirred at 2,000 rpm at 70 °C for 1 h. The colloidal galactomannan-coated magnetic Fe_3O_4 nanoparticles were washed with

deionized water:ethanol solution in three stages at ratios of 50:50, 25:75, and 0:100. These were dehydrated with acetone and dried in an oven at 50 ºC for 12 h. All samples were stored at room temperature.

Characterization of nanoparticles

Fourier Transform-infrared spectroscopy (FT-IR) was conducted with a Model Vertex instrument (Bruker, Ettlingen, Germany). The spectra were recorded in the attenuated total reflectance (ATR) mode by averaging 32 scans at a spectral range from 4000 to 400 cm^{-1} and a resolution of 4 cm^{-1}.

X-ray diffraction (XRD) characterization was achieved with a Rigaku Model RU 200R diffractometer (Rigaku Corp., Tokyo, Japan), using a Cu Kα (λ = 1.54 Å) x-ray at 30 kV and 30 mA in the angular range 2θ = 25° - 70°, and a step size of 2 °.min^{-1}.

A JSM 6701F field-emission scanning electron microscope (FEG-SEM, JEOL, USA) was used to obtain micrographs of nanoparticles. Average nanoparticle diameters were measured using the ImageJ software (National Institutes of Health, Bethesda, MD, USA) from at least 100 measurements of randomly selected nanoparticles.

Thermogravimetric analysis (TGA) was conducted on the Gal, FeNP, and FeNP/Gal samples using an analyzer from TA Instruments, model TGA Q500 V6.7 Build 203 (New Castle, DE, USA). Approximately 10 mg of each sample was placed in a platinum pan heated over a temperature range of 25-700 °C at 10 °C.min^{-1} under an oxidative atmosphere (60:40 N_2/air).

Biological activity

Cell culture

The strain used for the cytotoxicity assay was HEK-293 (ATCC® CRL-1573) from human embryo renal cells. The cells were cultured in 250-mL flasks with Dulbecco's

Modified Eagle Medium (DMEM) from Thermo Fisher Scientific (Waltham, MA, USA) supplemented with 10% fetal bovine serum and 1% solution of antibiotics (penicillin 100 U.mL^{-1} and streptomycin 100 µg.mL^{-1}) obtained from Sigma Aldrich Company (Milwaukee, WI, USA). The cells were incubated in a CO_2 oven at 37 ºC with an atmosphere of 5% CO_2 and 95% humidity and periodically observed with the aid of an inverted microscope.

Cytotoxicity assay with Alamar Blue (resazurin)

The alamar blue assay was used to assess the cell viability of HEK-293 cells (obtained from the Cell Bank of Rio de Janeiro, RJ, Brazil) against FeNP and FeNP/Gal samples. The cells in logarithmic growth were seeded in 96-well plates at a density of 10^5 cells.mL^{-1}. Then 100 µL.well^{-1} were applied and incubated for 24 h in an oven with an atmosphere of 5% CO_2, 95% relative humidity under 37 °C.

The FeNP and FeNP/Gal nanoparticles were autoclaved at 121 °C for 15 min to rule out microbiological contamination. 1 µL of the stock solution of each sample was removed and diluted directly in a serial manner in the complete DMEM medium. The tested concentrations ranged from 12.5 to 800 µg.mL^{-1}. Cell viability control (CTL) was represented by the complete culture medium. Wells containing only medium and sample were evaluated for possible interference with the fluorescence reading. After applying the samples, the plates were incubated at 37 °C for 72 h, with an atmosphere of 5% CO_2 and 95% humidity. In addition, before the end of the incubation period, 10 µL of the 0.312 mg.mL^{-1} Alamar Blue solution (Sigma-Aldrich, San Louis, Missouri, USA) was added to each well. After a fixed time, the fluorescence was measured with the aid of the ELISA reader (BioTek Synergy HT, UK) using an excitation wavelength at 530-560 nm and emission at 590 nm. Cell viability (%) was calculated using Equation (1):

$$Viability\ (\%) = \left(\frac{RFU_{treated}}{RFU_{control}}\right) \times 100 \qquad (1)$$

where $RFU_{treated}$ corresponds to the relative fluorescence units of the wells treated with the samples, and $RFU_{control}$ to the relative fluorescence units of the untreated wells.

Statistical analysis

For cytotoxicity, samples were tested in serial dilutions in triplicate, and the results were evaluated according to the mean ± standard error of the mean (E.P.M.) of the percentage of cell growth inhibition of *n* independent experiments. The data were analyzed by two-way ANOVA using the GraphPad Prism Software, version 7.03.

Supporting Information

Supporting information text

Supporting Information File 1: SUPPLEMENTARY MATERIAL

File Name: SUPPLEMENTARY MATERIAL

File Format: .Docx file was attached as Supplementary Material. It contains the NMR data which are cited in Figures S1-S2.

Figure S1: ^{1}H NMR of the galactomannan.

Figure S2: ^{1}H-^{13}C HSQC spectrum of the galactomannan.

Acknowledgements

We acknowledge Centro Nacional de Biologia Estrutural e Bioimagem (CENABIO) for the access to perform the NMR analysis and Dr. K.T. Klasson for helpful discussions. This research was supported in part by the U.S. Department of Agriculture, Agricultural Research Service. Mention of trade names or commercial products in this publication is solely for the purpose of providing specific information and does not imply recommendation or endorsement by the U.S. Department of Agriculture. USDA is an equal opportunity provider and employer.

Funding

Thanks are due to the funders of this research, including Capes, CNPq, Funcap, Finep, the National Nanotechnology Laboratory Applied to Agribusiness - Embrapa Instrumentation - São Carlos / SP and Embrapa Agroindústria Tropical, and the Technological Chemistry Laboratories and Microbiological Control Laboratory at the University of Fortaleza.

References

1. Sun, K.; Sun, C.; Tang, S. *CrystEngComm* **2016**, *18* (5), 714-720, 10.1039/C5CE02095F.

2. Lan, J.; Chen, J.; Li, N.; Ji, X.; Yu, M.; He, Z. *Talanta* **2016**, *151*, 126-131.

3. Wang, W.; Li, Q.; Zheng, A.; Li, X.; Pan, Z.; Jiang, J.; Zhang, L.; Hong, R.; Zhuang, L. *Results Phys.* **2019**, *14*, 102366.

4. Rahman, M. M.; Asiri, A. M. *Sensing and Bio-Sensing Research* **2015**, *4*, 109-117.

5. Ezzaier, H.; Marins, J. A.; Claudet, C.; Hemery, G.; Sandre, O.; Kuzhir, P. *Nanomaterials* **2018**, *8* (8).

6. Catalano, E.; Di Benedetto, A. *J. Phys. Conf. Ser.* **2017**, *841*, 012010.

7. Albarqi, H. A.; Wong, L. H.; Schumann, C.; Sabei, F. Y.; Korzun, T.; Li, X.; Hansen, M. N.; Dhagat, P.; Moses, A. S.; Taratula, O.; Taratula, O. *ACS Nano* **2019**, *13* (6), 6383-6395.

8. Lorenzi, H.; Matos, F. J. A. *Plantas Medicinais no Brasil: nativas e exóticas cultivadas* Instituto Plantarun de Estudos da Flora Ltda.: Brazil - Nova Odessa, SP, 2002.

9. Braga, R. C.; Teixeira-Sá, D. M. A.; Ribeiro, A. F.; Miranda, R. L.; Almeida, L. M. D.; Horta, A. C. G.; Moreira, R. D. A. *Braz. Arch. Biol. Technol.* **2011**, *54* (2), 283-292.

10. Cerqueira, M. A.; Souza, B. W. S.; Teixeira, J. A.; Vicente, A. A. *Food Hydrocoll.* **2012**, *27* (1), 175-184.

11. Mendes, F. R. S.; Bastos, M. S. R.; Mendes, L. G.; Silva, A. R. A.; Sousa, F. D.; Monteiro-Moreira, A. C. O.; Cheng, H. N.; Biswas, A.; Moreira, R. A. *Food Hydrocoll.* **2017**, *70*, 181-190.

12. De Sousa, F. D.; Holanda-Araújo, M. L.; Roberto, J.; De Souza, R.; Miranda, R. D. S.; Almeida, R. R.; Gomes-filho, E.; Pontes-Ricardo, N. M.; Monteiro-Moreira, A. C. O.; Moreira, R. D. A. *Open Access Library Journal* **2017**, *4*, e3683.

13. Silveira, J. L. M.; Bresolin, T. M. B. *Quim. Nova* **2011**, *34* (2), 292-299.

14. Frota, H. B. M.; Menezes, J.; Siqueira, S.; Ricardo, N.; Araújo, T.; Souza, C.; Bandeira, P.; Santos, H. *Quim. Nova* **2018**, *41* (5), 544-549.

15. Jeevanandham, S.; Dhachinamoorthi, D.; Sekhar, K. B. C. *Iran. J. Pharm. Sci.* **2011**, *Volume 10* (Number 3), 597-603.

16. de Sousa, F. D.; Vasconselos, P. D.; da Silva, A. F. B.; Mota, E. F.; da Rocha Tomé, A.; Mendes, F. R. d. S.; Gomes, A. M. M.; Abraham, D. J.; Shiwen, X.; Owen, J. S.; Lourenzoni, M. R.; Campos, A. R.; Moreira, R. d. A.; Monteiro-Moreira, A. C. d. O. *Int. J. Biol. Macromol.* **2019**, *121*, 429-442.

17. Sousa, A. M. M.; Gonçalves, M. P. *Carbohydr. Polym.* **2015**, *132*, 196-204.

18. Souza, N. D. G.; Freire, R. M.; Cunha, A. P.; da Silva, M. A. S.; Mazzetto, S. E.; Sombra, A. S. B.; Denardin, J. C.; Ricardo, N. M. P. S.; Fechine, P. B. A. *MCP* **2015**, *156*, 113-120.

19. Cerqueira, M. A.; Pinheiro, A. C.; Souza, B. W. S.; Lima, Á. M. P.; Ribeiro, C.; Miranda, C.; Teixeira, J. A.; Moreira, R. A.; Coimbra, M. A.; Gonçalves, M. P.; Vicente, A. A. *Carbohydr. Polym.* **2009**, *75* (3), 408-414.

20. Cerqueira, M. A.; Lima, Á. M.; Teixeira, J. A.; Moreira, R. A.; Vicente, A. A. *J. Food Eng.* **2009**, *94* (3), 372-378.

21. Bento, J. F.; Mazzaro, I.; de Almeida Silva, L. M.; de Azevedo Moreira, R.; Ferreira, M. L. C.; Reicher, F.; de Oliveira Petkowicz, C. L. *Carbohydr. Polym.* **2013**, *92* (1), 192-199.

22. Silverstein, R. M. *Spectrometric Identification of Organic Compounds*, 8th Revised ed. ed.; John Wiley & Sons: 2005.

23. Ebrahiminezhad, A.; Ghasemi, Y.; Rasoul-Amini, S.; Barar, J.; Davaran, S. *Bull. Korean Chem. Soc.* **2012**, *33* (12), 3957-3962.

24. Ruíz-Baltazar, A.; Esparza, R.; Rosas, G.; Pérez, R. *J. Nanomater.* **2015**, *2015*, 240948.

25. El-Guendouz, S.; Aazza, S.; Lyoussi, B.; Bankova, V.; Lourenço, J. P.; Costa, A. M. R.; Mariano, J. F.; Miguel, M. G.; Faleiro, M. L. *Molecules* **2016**, *21* (9).

26. Cerqueira, M. A.; Souza, B. W. S.; Simões, J.; Teixeira, J. A.; Domingues, M. R. M.; Coimbra, M. A.; Vicente, A. A. *Carbohydr. Polym.* **2011**, *83* (1), 179-185.

27. Pascoal, K. L. L.; Siqueira, S. M. C.; de Amorim, A. F. V.; Ricardo, N. M. P. S.; de Menezes, J. E. S. A.; da Silva, L. C.; de Araújo, T. G.; Almeida-Neto, F. W. Q.; Marinho, E. S.; de Morais, S. M.; Saraiva, G. D.; de Lima-Neto, P.; dos Santos, H. S.; Teixeira, A. M. R. *J. Mol. Struct.* **2021**, *1239*, 130499.

28. Kurt, A.; Kahyaoglu, T. *Carbohydr. Polym.* **2014**, *104*, 50-58.

29. Sato, M. D. F.; Rigoni, D. C.; Canteri, M. H. G.; Petkowicz, C. L. D. O.; Nogueira, A.; Wosiacki, G. *Acta Sci. Agron.* **2011**, *33* (3).

30. Figueiró, S. D.; Góes, J. C.; Moreira, R. A.; Sombra, A. S. B. *Carbohydr. Polym.* **2004**, *56* (3), 313-320.

31. *NIST, NIST Standard Reference Database Number 69*; 2016.

32. Kalasinsky, V. F.; Wurrey, C. J. *JRSp* **1980**, *9* (5), 315-323, https://doi.org/10.1002/jrs.1250090509.

33. Wang, F.; Polavarapu, P. L. *J. Phys. Chem. A* **2000**, *104* (26), 6189-6196.

34. Ertürk, E.; Göllü, M.; Demir, A. S. *Tetrahedron* **2010**, *66* (13), 2373-2377.

35. Jat, J. L.; Kumar, G. *Adv. Synth. Catal.* **2019**, *361* (19), 4426-4441, https://doi.org/10.1002/adsc.201900392.

36. Ali, A. A. A.; Hsu, F.-T.; Hsieh, C.-L.; Shiau, C.-Y.; Chiang, C.-H.; Wei, Z.-H.; Chen, C.-Y.; Huang, H.-S. *Sci. Rep.* **2016**, *6* (1), 36650.

37. Unterweger, H.; Subatzus, D.; Tietze, R.; Janko, C.; Poettler, M.; Stiegelschmitt, A.; Schuster, M.; Maake, C.; Boccaccini, A.; Alexiou, C. *Int. J. Nanomedicine* **2015**, 6985.

38. Lim, J.; Yeap, S. P.; Che, H. X.; Low, S. C. *Nanoscale Res. Lett.* **2013**, *8* (1), 381.

39. McGrath, A. J.; Dolan, C.; Cheong, S.; Herman, D. A. J.; Naysmith, B.; Zong, F.; Galvosas, P.; Farrand, K. J.; Hermans, I. F.; Brimble, M.; Williams, D. E.; Jin, J.; Tilley, R. D. *JMMM* **2017**, *439*, 251-258.

40. Gaber, A.; Abdel- Rahim, M. A.; Abdel-Latief, A. Y.; Abdel-Salam, M. N. *Int. J. Electrochem. Sci.* **2014**, *9*, 81-95.

41. Jadhav, S. V.; Nikam, D. S.; Mali, S. S.; Hong, C. K.; Pawar, S. H. *New J. Chem.* **2014**, *38* (8), 3678-3687, 10.1039/C4NJ00334A.

42. Vargas, M. A.; Diosa, J. E.; Mosquera, E. *Data in Brief* **2019**, *25*, 104183.

43. Mos, Y. M.; Vermeulen, A. C.; Buisman, C. J. N.; Weijma, J. *GeomJ* **2018**, *35* (6), 511-517.

44. Huff, W. D. *Clays Clay Miner.* **1990**, *38* (4), 448-448.

45. Sarkar, A.; Sil, P. C. *Food Chem. Toxicol.* **2014**, *71*, 106-115.

563 46. Andrade, A. L.; Souza, D. M.; Pereira, M. C.; Fabris, J. D.; Domingues, R. Z.
564 *Cerâmica* **2009**, *55* (336), 420-424.

565 47. Gao, S.; Shi, Y.; Zhang, S.; Jiang, K.; Yang, S.; Li, Z.; Takayama-Muromachi,
566 E. *J. Phys. Chem. C* **2008**, *112* (28), 10398-10401.

567 48. Díaz-Hernández, A.; Gracida, J.; García-Almendárez, B. E.; Regalado, C.;
568 Núñez, R.; Amaro-Reyes, A. *J. Nanomater.* **2018**, *2018*, 9468574.

569 49. Vendruscolo, C. W.; Ferrero, C.; Pineda, E. A. G.; Silveira, J. L. M.; Freitas, R.
570 A.; Jiménez-Castellanos, M. R.; Bresolin, T. M. B. *Carbohydr. Polym.* **2009**, *76*
571 (1), 86-93.

572 50. Mishra, D.; Arora, R.; Lahiri, S.; Amritphale, S. S.; Chandra, N. *Prot. Met. Phys.*
573 *Chem. Surf.* **2014**, *50* (5), 628-631.

574 51. Mudgil, D.; Barak, S.; Khatkar, B. S. *Int. J. Biol. Macromol.* **2012**, *50* (4), 1035-
575 1039.

576 52. Hongbo, T.; Yanping, L.; Min, S.; Xiguang, W. *Polym. J.* **2012**, *44* (3), 211-216.

577 53. Abruzzi, R. C.; Dedavid, B. A.; Pires, M. J. R. *Cerâmica* **2015**, *61* (359), 328-
578 333.

579 54. Hoque, M. A.; Ahmed, M. R.; Rahman, G. T.; Rahman, M. T.; Islam, M. A.; Khan,
580 M. A.; Hossain, M. K. *Results Phys.* **2018**, *10*, 434-443.

581 55. Assa, F.; Jafarizadeh-Malmiri, H.; Ajamein, H.; Anarjan, N.; Vaghari, H.; Sayyar,
582 Z.; Berenjian, A. *Nano Res.* **2016**, *9* (8), 2203-2225.

583 56. Pankhurst, Q. A.; Connolly, J.; Jones, S. K.; Dobson, J. *J. Phys. D: Appl. Phys.*
584 **2003**, *36* (13), R167-R181.

57. Bárcena, C.; Sra, A. K.; Gao, J. Applications of Magnetic Nanoparticles in Biomedicine. In *Nanoscale Magnetic Materials and Applications*; Liu, J. P.; Fullerton, E.; Gutfleisch, O.; Sellmyer, D. J., Eds.; Springer US: Boston, MA, 2009; pp 591-626.

58. Koedrith, P.; Boonprasert, R.; Kwon, J. Y.; Kim, I.-S.; Seo, Y. R. *Mol. Cell. Toxicol.* **2014**, *10* (2), 107-126.

59. Dissanayake, N. M.; Current, K. M.; Obare, S. O. *Int. J. Mol. Sci.* **2015**, *16* (10).